JOURNAL OF GEOPHYSICAL RESEARCH, VOL. 100, NO. D8, PAGES 16,265–16,273, AUGUST 20, 1995

Simulation of summer snowmelt on the Greenland ice sheet using a one-dimensional model

Clinton M. Rowe and Karl C. Kuivinen

Meteorology/Climatology Program, Department of Geography, and Snow and Ice Research Group, University of Nebraska-Lincoln

Rachel Jordan

Geophysical Sciences Branch, U.S. Army Cold Regions Research and Engineering Laboratory, Hanover, New Hampshire

Abstract. A one-dimensional heat and mass balance model of a snowpack over frozen soil was modified for use in glacial environments. The model solves a set of governing equations for the energy and mass balances of the snow, subject to observed meteorological conditions at the upper boundary and the assumption of a steady state at the lower boundary. The initial state of the snowpack is defined by the temperature, density and grain size profiles at the beginning of the simulation period. The data used to test the model on the Greenland ice sheet are a subset of the meteorological and surface data collected during the 1990 summer field season by the Swiss Federal Institute of Technology (ETH) Greenland Expedition. The site was located near the equilibrium line elevation on the west slope of the ice sheet. The relatively large amount of snowmelt experienced at this site during the summer of 1990 provides a robust test of the snowmelt model. Both the simulated height and mass of the snowpack agree well with the observations. The evolution of profiles of temperature, density and liquid water content also conform to our expectations of the physical changes taking place in the snowpack during melt. Results from the present model are also compared to those from a similar model and differences between the models are discussed.

Introduction

The Greenland ice sheet exerts an influence on the atmosphere, at least at a regional scale, due to the combined effects of its elevation, surface temperature and albedo. In turn, the mass balance of the ice sheet depends on the relationship between the ice sheet and its climatic environment, especially in terms of the mass and energy exchanges that take place at the surface of the ice sheet. Simply stated, the average net mass balance of the entire ice sheet is determined by evaluating the difference between accumulation and ablation at many individual points throughout the entire area. However, the response of the ice sheet to natural or human-induced variations in climate is incompletely understood due to the complex interactions between the ice sheet and the atmosphere at various spatial and temporal scales. For example, a warming of the atmosphere over Greenland would be expected to increase ablation from the ice sheet resulting in a negative mass balance [*Van der Veen*, 1987; *Braithwaite*, 1990; *Braithwaite and Olesen*, 1990a; *Warrick and Oerlemans*, 1990; *Huybrechts et al.*, 1991]. Increased ablation would be due not only to increased sensible heat and longwave radiation fluxes to the ice sheet resulting in greater melt, but also to an increase in the area of the ablation zone and to a longer melt season. However, the increase in atmospheric water vapor that would accompany the temperature rise could result in increased precipitation over all or part of the ice sheet, partially or completely offsetting the increased ablation [*Van der Veen*, 1987; *Warrick and Oerlemans*, 1990; *Huybrechts et al.*, 1991].

Paper number 95JD01384
0148-0227/95/95JD-01384$05.00

Many studies of the mass balance of the Greenland ice sheet have parameterized ablation as a function of temperature, either alone or in combination with other variables such as wind speed [*Braithwaite*, 1990; *Huybrechts et al.*, 1991; *Reeh*, 1991]. For estimation of the current mass balance of the ice sheet, these parameterizations appear to be adequate, but they are inappropriate for the investigation of ice sheet mass balance in a changing climate. This is because of feedbacks between the ice sheet and the climate system that are not considered explicitly by the parameterizations and because the parameterizations might not remain valid under a changed climate due to extrapolation errors. Furthermore, because air temperature is a state variable, it will respond not only to changes in the climate, but also to any changes to the ice sheet itself.

Energy balance and degree-day models that incorporate the physics of snowmelt and reliable measurements of ice thickening and thinning rates can provide insight into the ice processes that might be affected by climate change [*Braithwaite*, 1990; *Braithwaite and Olesen*, 1990a,b]. It is the purpose of this investigation to employ an energy balance model to investigate the processes affecting mass balance at a specific site near the equilibrium line elevation [*Ohmura et al.*, 1991]. For this study, a one-dimensional model of snowpack physics that was originally developed at the Army Corps of Engineers Cold Regions Research and Engineering Laboratory (CRREL) [*Jordan*, 1991] has been employed. This model originally was formulated to consider snow over frozen ground, so that only a few modifications were necessary to implement the model for the case of interest (i.e., snow over firn/ice). The model solves a set of governing equations for the energy and mass balances of the snow, subject to observed meteorological conditions at the upper boundary and the assumption of a steady state at the lower boundary, from an initial state defined by the temperature, density and grain size profiles at the beginning of the simulation period.

Model Summary

General Methodology

The one-dimensional mass and energy balance model used in this study (SNTHERM) was developed for predicting temperature profiles within layered frozen media. It was partially based on the earlier work of *Anderson* [1976] and is similar in many respects to other recent mass and energy balance models for snow [*Akan*, 1984; *Bader and Weilenmann*, 1992; *Brun*, 1989; *Greuell and Oerlemans*, 1986; *Illangasekare et al.*, 1990; *Jordan*, 1983; *Loth*, 1993; *Morris*, 1987]. In addition to temperature prediction, SNTHERM simulates the various physical and hydrological processes within a snow cover, including water flow, compaction, grain growth, snow ablation, and snow accumulation. Only thermal processes are modeled for soil layers, and therefore a sink is included at the snow-soil interface which artificially drains infiltrating water when it reaches the soil. The snow or soil layers are modeled as mixtures of five constituents: dry soil material, dry air, ice, liquid water, and water vapor, denoted by the subscripts *d*, *a*, *I*, *l*, and *v*, respectively. The partial or bulk density (γ_k) of each constituent k is related to its intrinsic density (ρ_k) as

$$\gamma_k = \theta_k \rho_k , \tag{1}$$

where θ_k is the fractional volume. For this study of snow ablation over an ice sheet, it was possible, with minor modifications to the model, to treat the ice as a soil layer with no dry soil component, as indicated in Figure 1. This procedure made advantageous use of the intralayer drain in the model and avoided problems of ponding water, which are not handled in SNTHERM. To be succinct, references to the dry soil fraction are omitted from the equations in the following summary.

SNTHERM uses a control volume numerical procedure to describe the spatial domain [*Patankar*, 1980] and a Crank-Nicholson weighting scheme for the time domain. The conceptual grid used in the numerical solution is shown in Figure 1. In order to accommodate compaction of the snow cover, the control volume thickness is allowed to change over time. This is not the usual practice, but is efficient numerically since the control volume boundaries remain coincidental with the stratigraphy of the evolving snow cover. The mass of ice and water is assumed to be conserved under contraction of the control volume, whereas the displaced portion of air and water vapor are expelled. Governing sets of equations are linearized with respect to the unknown variables and solved by the Thomas or tridiagonal matrix algorithm (TDMA) [*Patankar*, 1980]. For each time step, the mass balance equations are solved first and the water flux and snow density from this computation are used in the subsequent solution of the energy equation. Readers desiring further details on the numerical methods of SNTHERM or on the governing equations are referred to *Jordan* [1991].

Conservation Equations

One-dimensional mass balance equations for the total snow medium and the three water constituents, respectively, are of the form

$$\frac{\partial}{\partial t}\int \rho_s dz = - \sum_{k=i,v} \sum_{S} \boldsymbol{J}_k \cdot \boldsymbol{n} \tag{2}$$

and

$$\frac{\partial}{\partial t}\int \gamma_k dz = -\sum_{S} \boldsymbol{J}_k \cdot \mathbf{n} + \sum_{k'=i,l,v} \int M_{kk'}\, dz (1-\delta_{k'k}) \tag{3}$$

where t is time, ρ_s is the overall snow density, z is the vertical position relative to the snow-soil interface, dz is the incremental control volume thickness, $\boldsymbol{J}_k$ is the flux of water constituent k (positive upwards), $\mathbf{n}$ is a unit vector normal to the surface of the control volume, and $\sum_S$ indicates a summation over the top and bottom surfaces of the control volume. The source terms M_{li}, M_{vl} and M_{vi} are the mass rates of melt, evaporation, and sublimation, respectively, $\delta_{kk'}$ is the Kronecker delta, and $M_{kk'} = -M_{k'k}$.

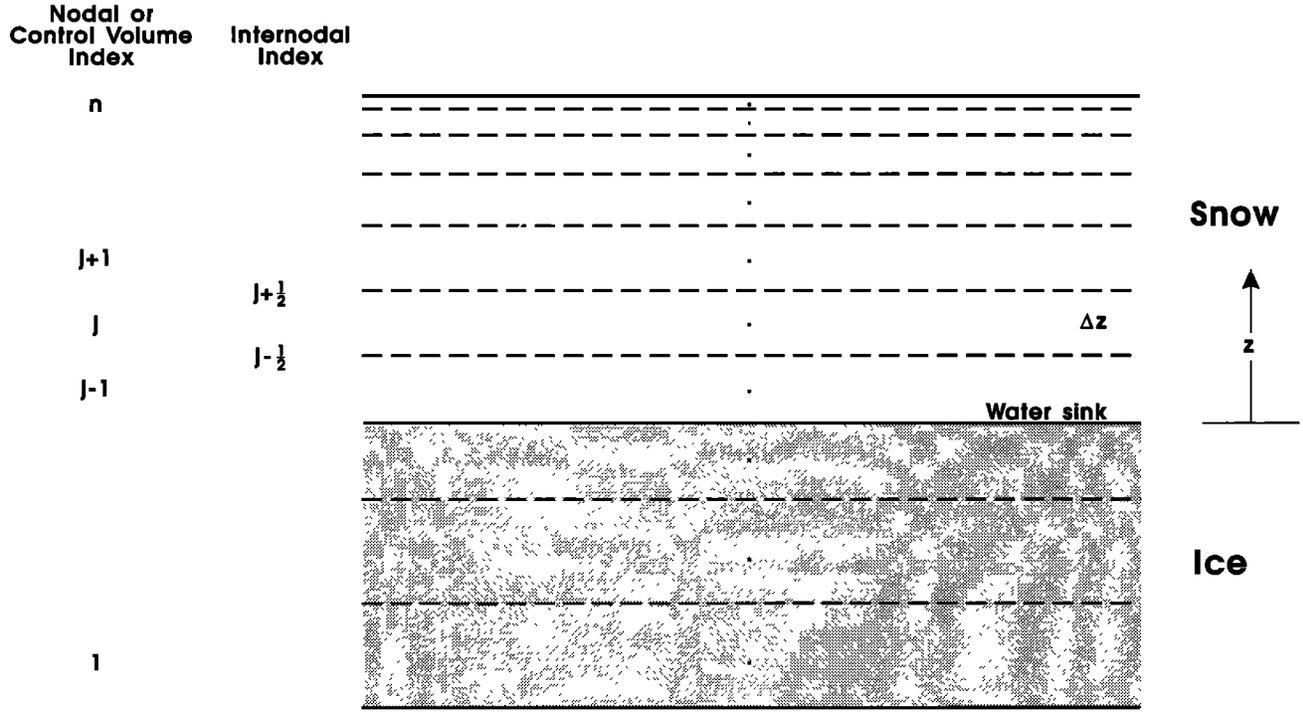

Figure 1. One dimensional grid for a two-layer system of snow over ice. The ice layer is treated as a soil without a dry soil component.

Air within the pore space is assumed to be stagnant and incompressible so that the vapor flux is driven by diffusion only. With the further assumption that the air is saturated, the vapor flux is computed from Fick's law as

$$J_v = -D_e \frac{\partial \rho_{v,sat}}{\partial z} = -D_e \frac{\partial \rho_{v,sat}}{\partial T} \frac{\partial T}{\partial z}, \quad (4)$$

where $\rho_{v,sat}$ is the intrinsic water vapor density at saturation, and D_e is an effective diffusion coefficient for vapor flow through snow which takes into account condensation and sublimation of vapor on the ice grains. Having specified that the control volume remains coincidental with the compacting snow cover, the mass flux of ice is taken as 0. Movement of liquid water through snow is assumed to be governed by Richards' equation [*Richards*, 1931]. Since capillary forces within snow are usually 2 to 3 orders of magnitude less than those of gravity [*Colbeck*, 1971], they are neglected, and the liquid water flux is expressed as

$$J_l = \frac{K_l}{\mu_l} \rho_l^2 g, \quad (5)$$

where K_l is the hydraulic permeability, g is the gravitational constant, ρ_l is the density of water, and μ_l is the dynamic viscosity of water. The formula of *Brooks and Corey* [1964] is used for estimating K_l

$$K_l = K_{max} s_e^{\epsilon}, \quad (6)$$

where s_e is the effective saturation $(s - s_r)/(1 - s_r)$, s is the liquid water saturation, s_r is the residual liquid water saturation, K_{max} is the saturated permeability computed from the formula of *Shimizu* [1970] and the parameter ϵ is taken as three [*Colbeck and Anderson*, 1982]. Discounting evaporative changes, the water flow equation is formulated from the equation for liquid water continuity as

$$\rho_l (1 - s_r) \frac{\partial}{\partial t} \int s_e \phi \, dz = \frac{\rho_l^2 g}{\mu_l} \sum_S (K_{max} s_e^3 \mathbf{k}) \cdot \mathbf{n} + \int M_{li} \Delta z \quad (7)$$

where $\mathbf{k}$ is a unit vector in the upwards vertical direction. The snow porosity ϕ changes with time and is related to M_{li} through the continuity equation for ice.

The water infiltration pattern generated by (7) consists of a step function in the vertical direction and even wetting in the horizontal direction. Whereas this simplified simulation of the flow pattern is adequate for many modeling purposes, it is important to note that it is not a realistic description. The actual flow pattern is almost always in the form of fingers, which disperse the leading edge of the infiltration wave and accelerate its arrival at the bottom of the snow cover [*Colbeck*, 1979; *Marsh and Woo*, 1984]. In addition, discontinuities in hydraulic permeability and capillary tension between heterogeneous snow layers result in horizontal flow along these textural boundaries. There is also an uncertainty associated with the selection of the residual saturation, since it must be satisfied prior to the advancement of the water front and therefore directly affects the infiltration rate. Moreover, the amount of water retained by the snowpack and the snow density are directly related to this parameter. A summary by *Kattelmann* [1986] on measurements of the residual water content ($\theta_r = s_r \phi$) shows a broad range of values from 0.0 to 0.4, with most lying between 0.01 and 0.05. A intermediate value of s_r=0.04 has been selected as the default value for the model.

The one-dimensional equation for the conservation of energy is written as

$$\frac{\partial}{\partial t} \int \rho_s h_s \, dz = -\sum_{k=l,v} \sum_S J_k h_k \cdot \mathbf{n} + \sum_S k_s \nabla T \cdot \mathbf{n} - \sum_S R_S \cdot \mathbf{n} \quad (8)$$

where h is the specific enthalpy taken with respect to the fusion point of water, k_s is the thermal conductivity of snow, and R_s is the net radiation. The general expression for enthalpy is

$$h = \int_{273.15}^{T} c(T) dT + L, \quad (9)$$

where c and L are the specific and latent heats, respectively. The first term in (8) represents the change in stored heat and the subsequent terms represent heat fluxes due to water flow, vapor diffusion, conduction, and solar radiation (R_S), respectively. Disregarding hysteresis effects, the unfrozen water content (γ_l) is related to temperature through an adaptation of the formula developed by *Guryanov* [1985] for soil

$$f_l = \frac{\gamma_l}{\gamma_w} = \frac{1}{1 + (a_1 T_D)^2}, \quad (10)$$

where T_D is the temperature depression (273.15 – T), and $\gamma_w = \gamma_l + \gamma_i$. A value of $a_1 = 100$ was selected to provide a reasonably sharp curve (99% of the water is frozen at -0.10°C) while avoiding the numerical difficulties associated with too steep a slope. Sensible and latent heat changes are combined in an apparent heat capacity (c_{app}) as

$$c_{app} = c_s + L_{li} \frac{\partial f_l}{\partial T} + L_{vi} \frac{\theta_v}{\gamma_w} \frac{\partial \rho_{v,sat}}{\partial T}, \quad (11)$$

where c_s is the specific heat of the total snow medium, and L_{li} and L_{vi} are the latent heats of fusion and sublimation, respectively.

The solar absorption term in (8) depends primarily on the intensity, angle, and spectral composition of the incident radiation, and on snow albedo, optical depth, and grain diameter. As a first approximation, incident solar energy is assumed diffuse and isotropic, and is divided at 1.12 μm into components corresponding roughly to the visible and to the near and midinfrared regions of the spectrum. Infrared radiation is assumed to be totally absorbed within the top node, and visible radiation to decay according to Beer's law, where the asymptotic bulk extinction coefficient β_∞ is computed from the formula of *Bohren and Barkstrom* [1974]

$$\beta_\infty = \frac{0.003795 \gamma_w}{\sqrt{d}}, \quad (12)$$

using a value of 0.003795 suggested by *Anderson* [1976]. A value of 0.78 is set as a default for the albedo of snow, and 55% of the net solar radiation is considered to be in the near and midinfrared wavebands.

Snow Cover Metamorphism

The deformation rate of the snow cover takes into account settling due to metamorphism, compaction under the sustained pressure of the snow overburden and loss of snow structure during active melt, giving

$$\frac{\partial}{\partial z} \frac{\partial z}{\partial t} = \left[\frac{\partial}{\partial z} \frac{\partial z}{\partial t} \right]_{metamorphism} + \left[\frac{\partial}{\partial z} \frac{\partial z}{\partial t} \right]_{overburden} + \left[\frac{\partial}{\partial z} \frac{\partial z}{\partial t} \right]_{melt}, \quad (13)$$

where the algorithms for the first two mechanisms follow *Anderson* [1976]. Mass losses for nodes undergoing melt are compensated by a reduction in the control volume thickness so that a constant ice density is maintained. In addition to compaction, water and vapor flows are factors in the overall densification of the snow cover. If a control volume mass or thickness falls below prescribed minimums, either through melt, sublimation, or compaction, it is automatically combined with a neighboring volume.

The grain growth function for dry snow is an adaptation of a formula used to predict growth by sintering in metals and ceramics [*Stephenson*, 1967; *Gow*, 1969]. This function is directly related to vapor flux which provides the necessary vapor source for growth and inversely related to particle size. There is a marked increase in grain growth within wet snow [*Colbeck*, 1982]. The growth function in this case is related to liquid water content and is again inversely related to grain size, with a maximum size set at 3 mm.

Boundary Conditions

Upper boundary conditions at the snow surface are prescribed by meteorologically determined fluxes of mass and energy. The surface energy flux (I) is expressed as

$$I = -R_s\downarrow(1-\alpha_s) - R_L\downarrow + R_L\uparrow + I_{sens} + I_{lat} + I_{conv}\ , \tag{14}$$

where $R_s\downarrow$ is the energy flux of downwelling solar radiation, α_s is the snow albedo, $R_L\downarrow$ and $R_L\uparrow$ are the energy fluxes of downwelling and upwelling longwave radiation, I_{sens} and I_{lat} are the turbulent fluxes of sensible and latent heat, and I_{conv} is the heat convected by rain or falling snow. Solar radiation is estimated from the three-layer insolation model of *Shapiro* [1982, 1987], and the downwelling longwave flux is computed from the formula of *Idso* [1981], with the addition of the Wachtmann correction [*Hodges et al.*, 1983]. The upwelling longwave flux is expressed as

$$R_L\uparrow = \varepsilon_s \sigma T_0^4 + (1-\varepsilon_s) R_L\downarrow\ , \tag{15}$$

where the first term on the right is the longwave emission from the snow as a function of the surface temperature (T_0) and the emissivity of the snow (ε_s) and the second term is reflected downwelling longwave radiation. A value of 0.97 is used for the snow emissivity [*Jordan et al.*, 1989]. The turbulent fluxes are given by [*Andreas and Murphy*, 1986]

$$I_{sens} = -\rho_a c_a C_H w (T_a - T_0) \tag{16}$$

and

$$I_{lat} = -L_v C_E w (\rho_{v,a} - \rho_{0v,sa})\ , \tag{17}$$

where ρ_a is the air density, c_a is the specific heat of air at constant pressure, C_H is the bulk transfer coefficient for sensible heat, C_E is the bulk transfer coefficient for latent heat, w is the wind speed and $\rho_{v,a}$ is the vapor density in air, which is computed using the relative humidity. The bulk transfer coefficients are taken as equal and, assuming neutral stability, are computed from the roughness length (z_0) as

$$C_{EN} = C_{HN} = \frac{k^2}{\left[\ln\left(\frac{Z}{z_0}\right)\right]^2}\ , \tag{18}$$

where Z is the observation height above the snow interface. For nonneutral atmospheric conditions, the standard stability adjustment is made to C_{EN} and C_{HN} [*Large and Pond*, 1982; *Jordan*, 1992].

Rainfall and the turbulent exchange of water vapor provide the upper boundary fluxes in the mass balance and water flow equations, where the vapor flux is computed as the turbulent flux of latent heat divided by L_v. Additional nodes are added on top of the snow cover when snowfall occurs, using a default density of 100 kg m^{-3} for the new snow.

As the bottom boundary condition for the energy equation, a constant temperature of -8.9°C is assumed at a depth of 10 m, since the 10 m temperature is nearly constant on an annual basis [*Paterson*, 1980]. No lower boundary is required for the water flow equation when the gravitational approximation is used.

Data

The data used to test the model on the Greenland ice sheet are a subset of the meteorological and surface data collected during the 1990 summer field season by the Swiss Federal Institute of Technology (ETH) Greenland Expedition [*Ohmura et al.*, 1991]. The site was located near the equilibrium line elevation on the west slope of the ice sheet (69°34′25.3″N, 49°17′44.1″W, 1175 m above sea level (asl)). This site was originally chosen because the location of the equilibrium line should be a sensitive indicator of the relationship between glacier mass balance and climate variations [*Ohmura et al.*, 1992]. For the purpose of the current research, the relatively large amount of snowmelt experienced at this site during the summer of 1990 provides a robust test of the snowmelt model. In addition, data from this site were used by *Greuell and Konzelmann* [1994] to optimize and test an energy and mass balance model. These two models are similar in some respects but have significant differences in their formulation, initialization, and use. Results from the present model will be compared to those of *Greuell and Konzelmann* [1994], and the differences between the models will be discussed below.

Meteorological Data

Meteorological data (air temperature, relative humidity, wind speed, cloud cover, and precipitation) at 6-hour intervals from the ETH site were published for the entire field season. A subset of the data from JD 163 (June 12) to JD 212 (July 31) was extracted from the ETH data for use with the snowmelt model. This period begins at the first observation with all of the data needed to run the snowmelt model, and ends soon after the snowpack has completely melted. Before using the published data, missing and invalid air temperature data were estimated from the preceding and following observations, and two obvious typographical errors in relative humidity were corrected. Because the model uses linear interpolation to estimate meteorological variables at model time steps between observations, it was thought necessary to preprocess the data to create an hourly meteorological data set for input to the model. Hourly air temperature, relative humidity, and wind speed were estimated from the published data using cubic spline interpolation. Because of the difficulty associated with interpolating cloud type, both cloud cover and cloud type were held constant over a 6-hour period centered on the observation (i.e., for the hour of observation, the 3 hours preceding and 2 hours following). Precipitation was distributed over the 6-hour period preceding the observation so as to preserve the correct 6-hour precipitation total. With the exception of days 167 and 168, all the precipitation fell as rain. The resulting hourly data were converted to the proper units for input into the snowpack model (Figure 2). Because detailed radiation data were not published in a format that could be used in the model, they were estimated using the algorithms provided in the SNTHERM code.

Snowpack Data

The snowmelt model requires initial vertical profiles of temperature, density, and grain diameter for the snowpack and the underly-

ing substrate. Temperature and density profiles were estimated from published figures for the ETH site [*Ohmura et al.*, 1991]. The ETH scientists measured snowpack temperatures at six depths (initially 0, 19, 38, 57, 76, and 95 cm above the snow/ice interface) using thermistors inserted approximately 50 cm horizontally into the wall of a pit, which was subsequently filled. Measurements were made at 0000, 0600, 1200 and 1800 UT daily. Englacial temperatures were measured daily using thermistors mounted on cables that were lowered into holes drilled into the ice. A total of six such cables were used by the ETH scientists in 1990 [*Greuell*, 1991b]. To initialize SNTHERM, the snowpack temperatures were estimated for 0000 UT on JD 163 (June 12), while englacial temperatures to 10 m were estimated for the previous day. Since englacial temperatures can be expected to vary only slowly at the beginning of the summer, this should not introduce any significant errors into the initial temperature profile.

Mass balance measurements were made by the ETH scientists 4 times per day using five stakes set into the snow approximately 10 m apart. These snowpack heights were averaged to give a value representative of the change in height of the snowpack. Once per day, generally around 1800 UT, vertical profiles of density and liquid water content were obtained from the wall of a pit dug into the snowpack. Several different methods were used by the ETH scientists to measure density. The values used to initialize SNTHERM were interpolated from a graph presenting the density profile as measured at 5 cm intervals with a 500 cm^3 cylinder inserted horizontally into the pit wall. Raw density measurements were corrected before plotting to correspond to density measurements made using a large cylinder vertically inserted into the snowpack. Density estimates could not be made for the first day of simulation, but were obtained for JD 167 (June 16). Again, in the absence of significant melt, this should not introduce significant initialization errors. Liquid water content estimates were calculated from measurements of the dielectric constant of the snow made concurrently with the density profiles.

The initial grain size profile was estimated from descriptions contained in the ETH report. The grain sizes used to initialize the model are comparable to those estimated as a function of density [*Anderson*, 1976].

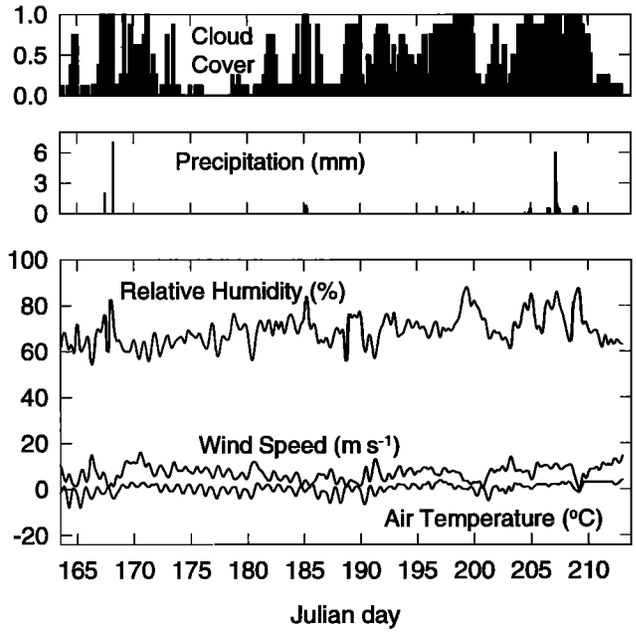

Figure 2. Meteorological conditions at the ETH site for input to the model.

Table 1. Snowpack Parameters Used in SNTHERM

Parameter	Default	Site-Specific
Roughness length (z_0)	0.007	0.001
Ratio of neutral stability bulk turbulent transfer coefficients of momentum and latent heat (C_{DN}/C_{EN})	1.5	1.0
Ratio of neutral stability bulk turbulent transfer coefficients of momentum and sensible heat (C_{DN}/C_{HN})	1.0	1.0
Windless exchange coefficient for latent heat (E_{E0})	0.0	0.0
Windless exchange coefficient for sensible heat (E_{H0})	1.8	1.0
Fractional humidity in snow (f_{rh})	1.0	1.0
Albedo (α)	0.78	0.70
Irreducible or residual liquid water saturation (s_r)	0.04	0.02

Results

Three model runs were made for a 50-day period from JD 163 (June 12) to JD 212 (July 31) 1990. The first run used the default snow properties (Table 1) given by *Jordan* (1990) for midlatitude seasonal snowpacks. This run left approximately 20 cm of snow on top of the ice at the end of the run, even though the actual snowpack had melted 2 days earlier (Figure 3). Most of the disagreement between the model and the observations arises from two periods (JD 176-178 and JD 186-189) when modeled mass loss occurs more slowly than observed.

The second run used snow properties chosen to be representative of the ETH site (Table 1). Roughness length was reduced to a value consistent with the relatively flat snow-covered terrain [*Arya*, 1988], the ratio of the turbulent transfer coefficients for latent heat and momentum was set to unity, the windless convection coefficient for sensible heat was set to zero, and the irreducible liquid water saturation was reduced by half. In terms of the mass balance, however, the most significant change was the reduction of the snow albedo from the default value to a value computed as a weighted average of the June and July monthly albedos reported by *Konzelmann* [1991] for the ETH site. Since the two periods of greatest discrepancy in the initial run were characterized by little or no cloud cover (Figure 2), the reduction in solar heating due to a too high albedo would be a likely cause. For this run, the height of the snowpack is reduced more rapidly than was the observed snowpack until just prior to the end of the run (Figure 3), and the modeled snowpack disappears less than 2 days after the observed. The mass of the snowpack is modeled closely until the last 5-6 days of the model run, when mass is removed too slowly. It must be noted that the observed mass was computed by *Greuell and Konzelmann* [1991] as the product of the snowpack height and an average snowpack density. Before JD 203 (July 22), they used as the density of snow a 5-day running mean of the density obtained by inserting the large cylinder vertically into the snowpack. From JD 203 to JD 210 (July 29), they used a constant snowpack density of 439 kg m^{-3} and after JD 210, a constant value of 300 kg m^{-3}. Ice lenses and slush were assumed to have densities of 900 kg m^{-3} and 950 kg m^{-3}, respectively. Therefore because of measurement errors

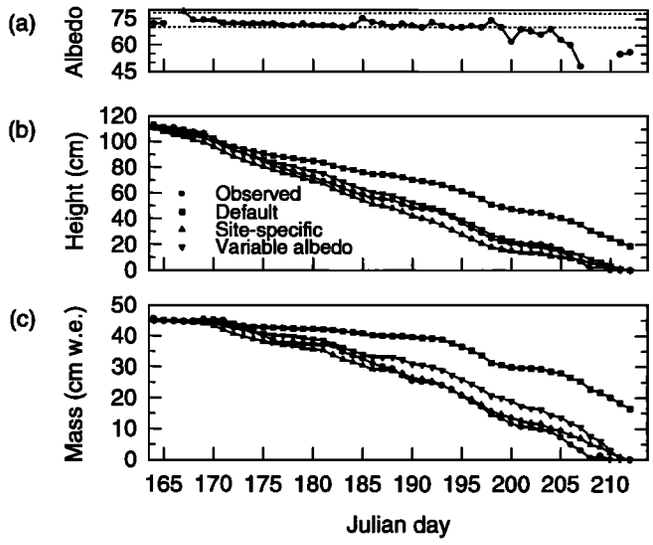

Figure 3. (a) Daily observed albedo (percent), with constant albedos used in runs 1 and 2 marked; (b) daily observed and modeled snowpack height (centimeters); and (c) daily observed and modeled snowpack mass balance (centimeters water equivalent).

and horizontal inhomogeneities, the observed mass balance may only be representative of the immediate area in which the measurements were taken (i.e., approximately 10 x 20 m), while the model results, based on the more spatially homogeneous climatic parameters, may actually represent more spatially averaged values.

Because the SNTHERM model assumes a constant albedo, the average albedo specified for the second run is initially too low, then becomes too high for the final 10-12 days of the run. This corresponds to the errors in the modeled mass balance, with mass being lost too quickly at the beginning of the run (i.e., absorption of solar radiation too high) and too slowly at the end of the run. To overcome this problem, a third run was performed in which the albedo was specified on a daily basis using observed values from *Greuell* [1991a]. This run gives better overall agreement with the observed snowpack height during the period than did the previous runs. However, the snowpack mass balance is not modeled as well as by the second run.

Further discussion of the evolution of the snowpack temperature, density and liquid water content profiles will be based on the results of the final model run using the site-specific snowpack properties and a variable albedo.

Snowpack Temperature

Both the actual and modeled snowpacks (Figure 4) become temperate (i.e., isothermal at 0°C) by JD 171 (June 20). The modeled snowpack (Figure 4b) remains essentially isothermal for the remainder of the simulation, but shows a diurnal variation in the upper 10-20 cm of the pack in response to the diurnal air temperature and radiation cycle.

Snowpack Density

Densities in the observed and simulated snowpacks (Figure 5) increase over time, as is expected, due to snow metamorphism. However, the density of the layer closest to the underlying ice becomes too high in the simulation, beginning about JD 175 (June 24) in the lowest 5 cm of the snowpack and growing to about 20 cm by JD 200 (July 19). This density increase is caused by liquid water from melt higher in the snowpack infiltrating and refreezing near the underlying ice and is responsible for much of the discrepancy between the simulated and observed mass. Once this dense layer forms, it reduces the infiltration rate of meltwater and continues to grow. Physically, this may be representative of the growth of superimposed ice as often occurs in the ablation zone of the ice sheet. Measurements of superimposed ice at the ETH camp indicated that it varied in thickness between 3 and 6 cm between JD 183 (July 2) and JD 202 (July 21) [*Greuell and Konzelmann*, 1991]. The actual snowpack at the ETH site, however, developed a slush layer beginning on JD 181 (June 30) that is not reproduced by the model since any liquid water reaching the ice surface is immediately drained away. If liquid water were allowed to accumulate in the lowest layers of the model snowpack, it would be more difficult for refreezing to occur and a slush layer could perhaps be formed. Slow drainage of liquid water from this slush layer would also improve the simulation of snowpack mass.

Snowpack Liquid Water Content

The bulk of the snowpack has volumetric liquid water content of 2-6% from JD 169 (June 18) through JD 197 (July 16) in both the observations and the simulation (Figure 6). In general, the simulated liquid water content is somewhat lower than the observed values, but since these measurements were made in the late afternoon, they may correspond more closely to daily maximum

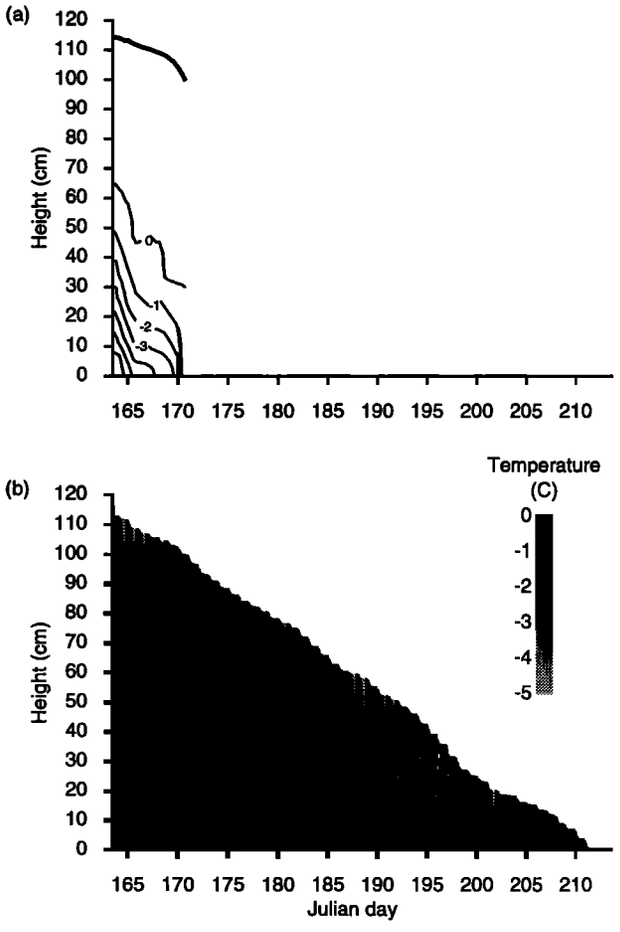

Figure 4. Time-height profile of (a) observed [adapted from *Greuell*, 1991b] and (b) modeled snowpack temperature (°C). The observed snowpack became isothermal at 0°C on JD 170 (June 19). The heavy line in (a) indicates the top of the snowpack.

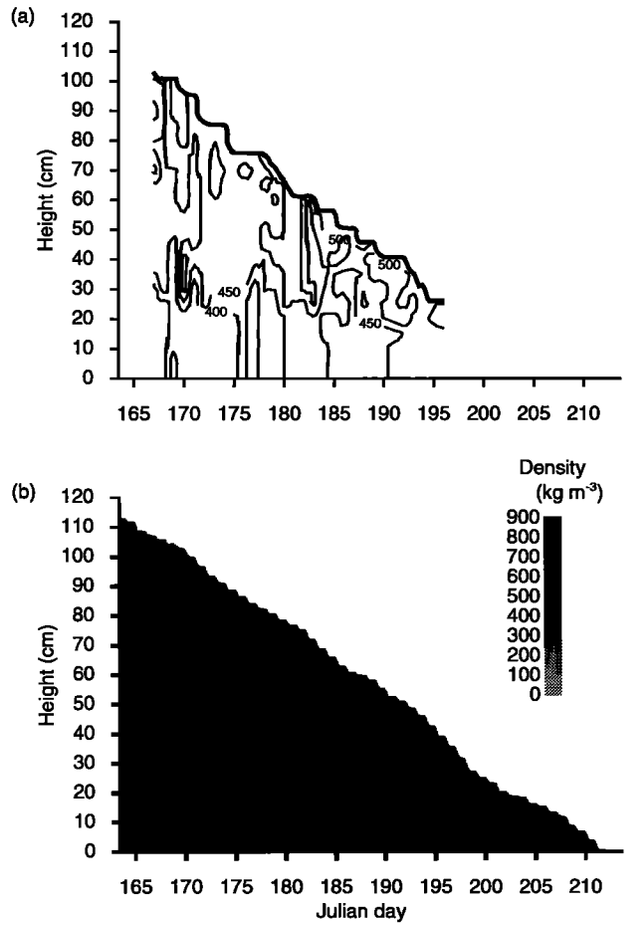

Figure 5. Time-height profile of (a) observed [adapted from *Greuell and Konzelmann*, 1991] and (b) modeled snowpack density (kilogram per cubic meter). Observed density profiles were not available after JD 196 (July 15). The heavy line in (a) indicates the top of the snowpack.

liquid water contents than to daily average values. In the simulated snowpack, liquid water content is higher above the denser snow layers since the rate of drainage through the snowpack largely is determined by the density of the snow. The lowest part of the simulated snowpack is too dry after about JD 175 (June 24). This is the same layer that became too dense at about the same time. The upper part of the snowpack, to depths of about 15-30 cm, experiences a diurnal cycle of liquid water content that corresponds to the melt/refreeze cycle in the upper portion of the snowpack.

Energy Fluxes

Time series of the daily energy fluxes between the snowpack and both the atmosphere and the underlying ice (Figure 7) show that sensible heat flux and net radiation are positive throughout the simulation. Thus these two terms provide the energy source for snowmelt, while latent heat flux and conduction into the ice are energy sinks and reduce the energy available for melt. Melt is more highly correlated with net radiation (r^2= 0.809) than with sensible heat flux (r^2= 0.076). This is contrary to the findings of Braithwaite and Olesen [*Braithwaite*, 1981; *Braithwaite and Olesen*, 1984, 1990b]. They attribute their results to the greater temporal variability, and therefore greater covariability with melt, of sensible heat flux as compared to net radiation. For this simulation, however, net radiation and sensible heat flux have nearly equal variance, but net radiation represents the larger energy source for melt and thus results in a greater temporal correlation.

Model Intercomparison

Greuell and Konzelmann [1994] present results of a numerical model of the surface energy and mass balance at the ETH site for 1990. As with SNTHERM, their model uses air temperature and humidity, wind speed, cloud amount, and precipitation as input. However, unlike SNTHERM, the parameterizations used in their model to compute the various flux terms were, for the most part, developed for the ETH site specifically or for Greenland. In addition, their simulations made use of measured, rather than computed, radiation fluxes. Two significant differences between the models are their (1) incorporation of a snow albedo parameterization based on density and cloud cover and (2) inclusion of a slush layer as compared to SNTHERM's prescribed albedo and free drainage.

Initial profiles of temperature, density and liquid water content were prescribed on JD 152 (June 1) as a uniform temperature of -8.8°C within the ice to a depth of 25 m and a linear increase from that value at the snow/ice interface to 0°C at the surface, a constant snowpack density of 380 kg m^{-3}, and dry snow (i.e., no liquid water present). They ran their model until JD 249 (September 6), resulting in the ablation of approximately 18 cm of ice.

Following an initial model run, Greuell and Konzelmann tuned the model to provide good agreement with the mass balance and

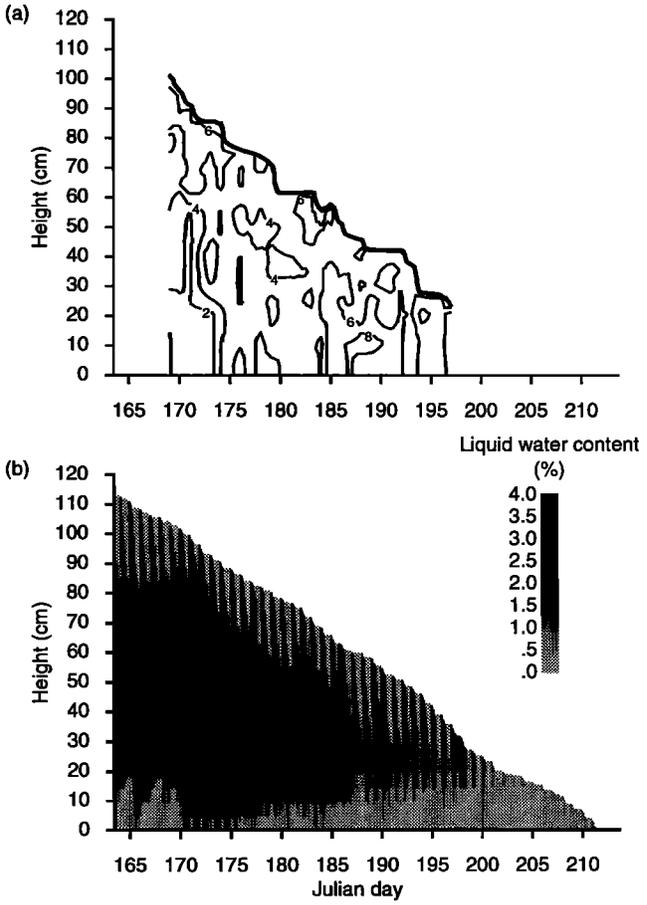

Figure 6. Time-height profile of (a) observed [adapted from *Greuell and Konzelmann*, 1991] and (b) modeled snowpack liquid water content (percent). Observed liquid water content profiles were not available after JD 197 (July 16). The heavy line in (a) indicates the top of the snowpack.

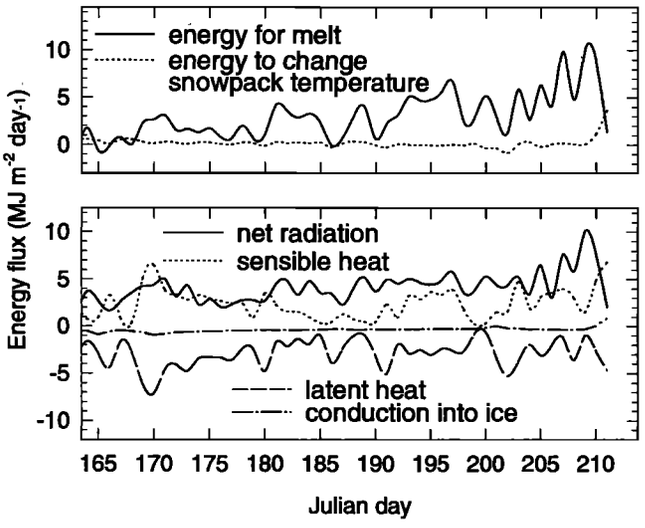

Figure 7. Time series of modeled energy fluxes at the surface of the snowpack.

englacial temperature profile by increasing the measured downward radiation fluxes by 0.5%, decreasing the reflected shortwave by a similar percentage and increasing the extinction coefficient for ice from 2.5 m^{-1} to 2.8 m^{-1}. These adjustment are, by their estimate, well within the respective uncertainties. As with SNTHERM, their simulated mass loss is delayed relative to the observed loss. They attribute this to their treatment of mass storage in the slush layer, which in their model is not allowed to drain until it has reached its capacity of 20 cm. Thus even though these models represent two extremes in their treatment of the drainage of meltwater from the snowpack, they both result in the retention of mass at the bottom of the snowpack.

Summary and Conclusions

SNTHERM, a one-dimensional energy and mass balance model developed at CRREL by *Jordan* [1992], was modified for use with snowpacks over ice. This model uses meteorological data and appropriate values for the surface properties to estimate the fluxes of shortwave and longwave radiation at the surface, sensible and latent heat transfers between the surface and the atmosphere, and the transfer of sensible heat into the snowpack. In addition, the profiles of temperature, density, grain size, thermal conductivity, specific heat, and liquid water content of the snowpack are estimated as the snowpack undergoes metamorphism over time.

Preliminary simulations were made using meteorological and snowpack data collected during the summer of 1990 at the Swiss camp near the equilibrium line on the west slope of the Greenland ice sheet [*Ohmura et. al.*, 1991]. Both the simulated height and mass of the snowpack agree well with the observations. Time-height profiles of temperature, density, and liquid water content conform to our expectations of the physical changes taking place in the snowpack during melt. Simulated snowpack temperatures show the nearly isothermal conditions characteristic of a melting snowpack, with the portion of the pack near the pack-ice interface remaining colder until the end of the simulated period. Small, diurnal variations in temperature are seen at the top of the snowpack in response to the diurnal fluctuations in net radiation, and sensible and latent heat fluxes. The rapid increase in density near the bottom of the snowpack is caused by meltwater from the upper levels of the snowpack freezing in the colder regions near the ice. The variation in liquid water content of the snowpack simulated by the model is essentially an inverse of the predicted bulk density since higher density layers in the snowpack have reduced pore space and, as a result, cannot hold as much liquid water as less dense layers.

Results from this type of simulation could be used to compute, for example, the onset and rate of snowmelt on the ice sheet. Since the emissivities of snow and liquid water are significantly different, especially in the microwave, these results may help to explain much of the temporal and spatial variation observed in passive microwave brightness temperatures over the ice sheet [*Mote et al.*, 1993; *Mote and Anderson*, 1994; *Mote and Rowe*, 1995].

Since exchanges of energy between the surface and the atmosphere determine the energy available to melt the snowpack, variations in surface properties, coupled with variations in cloud cover, atmospheric transmissivity and emissivity, and wind will contribute to spatial and temporal variations in the surface energy balance across the ice sheet and, therefore to variations in melt. We have begun to investigate which of the flux terms is responsible for most of the day-to-day variation in snowpack properties. Preliminary analysis of our simulation results shows that, as expected, net radiation provides the majority of the energy for ablation of the snowpack, with sensible heat supplying nearly all of the remainder. However, day-to-day variations in the amount of ablation seem to be highly correlated with the turbulent fluxes, implying that simple models of snowmelt based on correlations with air temperature may be able to capture much of the variance in snowmelt observed on the ice sheet. This result, when confirmed, will be important as we investigate the role of atmospheric circulation patterns on snowmelt over the ice sheet.

Acknowledgments. The authors would like to thank Mary R. Albert and Robert E. Davis, both of CRREL, and two anonymous reviewers for their helpful comments on earlier versions of this paper. This work was supported in part by NASA grant NAGW-1266 to the University of Nebraska-Lincoln.

References

Akan, A.O., Simulation of runoff from snow-covered hill slopes, *Water Resour. Res., 20*, 707-713, 1984.

Anderson, E. A., A point energy and mass balance model of a snow cover, *NOAA Tech. Rep. NWS 19*, Off. of Hydrol., Nat. Weather Serv., Silver Spring, Md., 1976.

Andreas, E. L., and B. Murphy, Bulk transfer coefficients for heat and momentum over leads and polynyas, *J. Phys. Oceanogr., 16*, 1875-1883, 1986.

Arya, S.P., *Introduction to Micrometeorology*, Academic, San Diego, Calif., 1988.

Bader, H.P., and P. Weilenmann, Modeling temperature distribution, energy and mass flow in a (phase-changing) snowpack, I, Model and case studies, *Cold Reg. Sci. Technol., 20*, 157-181, 1992.

Bohren, C., and B. Barkstrom, Theory of the optical properties of snow, *J. Geophys. Res., 79*, 4527-4535, 1974.

Braithwaite, R. J., On glacier energy balance, ablation, and air temperature, *J. Glaciol., 27*, 381-391, 1981.

Braithwaite, R. J., Greenland glaciers and the 'greenhouse effect,' *Rapp. Grønlands Geol. Unders., 148*, 51-53, 1990.

Braithwaite, R. J., and O. B. Olesen, Ice ablation in West Greenland in relation to air temperature and global radiation, *Z. Gletscherkd. Glazialgeol., 20*, 155-168, 1984.

Braithwaite, R. J., and O. B. Olesen, Increased ablation at the margin of the Greenland ice sheet under a greenhouse-effect climate, *J. Glaciol., 36*, 20-22, 1990a.

Braithwaite, R. J., and O. B. Olesen, Response of the energy balance on the margin if the Greenland ice sheet to temperature changes, *J. Glaciol., 36*, 217-221, 1990b.

Brooks, R. H., and A. T. Corey, Hydraulic properties of porous media, *Hydrology Papers, 3*, Colorado State Univ., Fort Collins, Colo., 1964.

Brun, E., E. Martin, V. Simon, C. Gendre, and C. Coleou, An energy and mass model of snow cover suitable for operational avalanche forecasting, *J. Glaciol., 35*, 333-342, 1989.

Colbeck, S. C., One-dimensional water flow through snow, *Research Report 296*, U. S. Army Corps of Eng., Cold Reg. Res. and Eng. Lab., Hanover, N. H., 1971.

Colbeck, S. C., Water flow through heterogeneous snow, *Cold Reg. Sci. Technol., 1*, 37-45, 1979.

Colbeck, S. C., and E.A. Anderson, The permeability of a melting snow cover, *Water Resour. Res., 18*, 904-908, 1982.

Gow, A. J., On the rates of grains and crystals in South Polar firn, *J. Glaciol., 8*, 241-252, 1969.

Greuell, W., Climatology, in *Energy and Mass Balance During the Melt Season at the Equilibrium Line Altitude, Paakitsoq, Greenland Ice Sheet: Progress Report 1*, edited by A. Ohmura, K. Steffen, H. Blatter, W. Greuell, M. Rotach, T. Konzelmann, M. Laternser, A. Ouchi, and D. Steiger, pp. 21-35, Dep. Geogr., Swiss Federal Inst. of Technol., Zurich, 1991a.

Greuell, W., Englacial temperature, in *Energy and Mass Balance During the Melt Season at the Equilibrium Line Altitude, Paakitsoq, Greenland Ice Sheet: Progress Report 1*, edited by A. Ohmura, K. Steffen, H. Blatter, W. Greuell, M. Rotach, T. Konzelmann, M. Laternser, A. Ouchi, and D. Steiger, pp. 76-82, Dep. Geogr, Swiss Federal Inst. of Technol., Zurich, 1991b.

Greuell, W., and T. Konzelmann, Mass budget, in *Energy and Mass Balance During the Melt Season at the Equilibrium Line Altitude, Paakitsoq, Greenland Ice Sheet: Progress Report 1*, edited by A. Ohmura, K. Steffen, H. Blatter, W. Greuell, M. Rotach, T. Konzelmann, M. Laternser, A. Ouchi, and D. Steiger, pp. 83-93, Dep. Geogr., Swiss Federal Inst. of Technol., Zurich, 1991.

Greuell, W., and T. Konzelmann, Numerical modelling of the energy balance and the englacial temperature of the Greenland Ice Sheet, Calculations for the ETH-Camp location (West Greenland, 1155 m a.s.l.), *Global Planet. Change, 9*, 91-114, 1994.

Greuell, W., and J. Oerlemans, Sensitivity studies with a mass balance model including temperature profile calculations inside the glacier, *Z. Gletscherkd. Glazialgeol., 22*, 101-124, 1986.

Guryanov, I. E., Thermal-physical characteristics of frozen, thawing and unfrozen grounds, in *Ground Freezing, Proceedings of the Fourth International Symposium on Ground Freezing*, edited by S. Kinosita and M. Fukuda, pp. 225-230, Hokkaido Univ. Press, Sapporo, Japan, 1985.

Hodges, D. B., G. J. Higgins, P. F. Hilton, R. E. Hood, R. Shapiro, C. N. Touart, and R. F. Wachtmann, Final tactical decision aid (FTDA) for infrared (8-12 μm) systems -- Technical background, *Sci. Rep. 5*, Syst. and Appl. Sci. Corp., Riverdale, Md., (under contract to Air Force Geophys. Lab., *Rep. AFGL-TR-83-0022*), 1983.

Huybrechts, P., A. Letreguilly, and N. Reeh, The Greenland ice sheet and greenhouse warming, *Palaeogeogr., Palaeoclim., Palaeoecol., 89*, 399-412, 1991.

Idso, S. B., A set of equations for full spectrum and 8-14 μm and 10.5-12.5 μm thermal radiation from cloudless skies, *Water Resour. Res., 17*, 295-304, 1981.

Illangasekare, T.H. and R.J. Walter Jr., M.F. Meier, and W.T. Pfeffer, Modeling of meltwater infiltration in subfreezing snow, *Water Resour. Res., 26*, 1001-1012, 1990.

Jordan, R., Meltwater movement in a deep snowpack, 2, Simulation model, *Water Resour. Res., 19*, 979-985, 1983.

Jordan, R., A one-dimensional temperature model for a snow cover: Technical documentation for SNTHERM.89, *Spec. Rep. 91-16*, U. S. Army Corps of Eng., Cold Reg. Res. and Eng. Lab., Hanover, N. H., 1991.

Jordan, R. Estimating turbulent transfer functions for use in energy balance models, *Internal Rep. 1107*, U. S. Army Corps of Eng., Cold Reg. Res. and Eng. Lab., Hanover, N. H., 1992.

Jordan, R., H. O'Brien, and M.R. Albert, Snow as a thermal background: Preliminary results from the 1987 field test, *Spec. Rep. 89-7*, U. S. Army Corps of Eng., Cold Reg. Research and Eng. Lab., Hanover, N. H., 1989.

Kattelman, R., Measurements of snow layer water retention, in *Proceedings of the Cold Regions Hydrology Symposium*, edited by D. L. Kane, pp. 377-386, American Water Resources Association, Bethesda, Md., 1986.

Konzelmann, T., Radiation measurements, in *Energy and Mass Balance During the Melt Season at the Equilibrium Line Altitude, Paakitsoq, Greenland Ice Sheet: Progress Report 1*, edited by A. Ohmura, K. Steffen, H. Blatter, W. Greuell, M. Rotach, T. Konzelmann, M. Laternser, A. Ouchi, and D. Steiger, pp. 51-59, Dep. Geogr., Swiss Federal Inst. of Technol., Zurich, 1991.

Large, W. G., and S. Pond, Sensible and latent heat flux measurements over the ocean, *J. Phys. Oceanogr., 12*, 464-482, 1982.

Loth, B., Snow cover model for global climate simulations, *J. Geophys. Res., 98*, 10,451-10,464, 1993.

Marsh, P., and M. K. Woo, Wetting front advance and freezing of meltwater within a snow cover, 1, Observations in the Canadian Arctic, *Water Resour. Res., 20*, 1853-1864, 1984.

Morris, E.M., Modeling of water flow through snowpacks, in *Seasonal Snow Covers: Physics, Chemistry, Hydrology*, edited by H.G. Jones and W.J. Orville-Thomas, pp. 179-208, D. Reidel, Dordrecht, 1987.

Mote, T.L., and M.R. Anderson, Variations in snowpack melt on the Greenland ice sheet based on passive-microwave measurements, *J. Glaciol. 41*, 51-60, 1995.

Mote, T.L., and C. M. Rowe, A comparison of microwave radiometric data and modeled snowpack conditions for Dye 2, Greenland, *Meteorology and Atmospheric Physics*, in press, 1995.

Mote, T.L., M.R. Anderson, K.C. Kuivinen, and C.M. Rowe, Passive microwave-derived spatial and temporal variations of summer melt on the Greenland ice sheet, *Ann. Glaciol., 17*, 233-238, 1993.

Ohmura, A., K. Steffen, H. Blatter, W. Greuell, M. Rotach, T. Konzelmann, M. Laternser, A. Ouchi, and D. Steiger, *Energy and Mass Balance During the Melt Season at the Equilibrium Line Altitude, Paakitsoq, Greenland Ice Sheet: Progress Report 1*, Dep. of Geogr., Swiss Federal Inst. of Technol., Zurich, 1991.

Ohmura, A., P. Kasser, and M. Funk, Climate at the equilibrium line of glaciers, *J. Glaciol., 38*, 397-411, 1992.

Patankar, S. V., *Numerical Heat Transfer and Fluid Flow*, Hemisphere, New York, 1980.

Paterson, W.S.B., Ice sheets and ice shelves, in *Dynamics of Snow and Ice Masses*, edited by S.C. Colbeck, pp. 1-78, Academic, New York, 1980.

Reeh, N., Parameterization of melt rate and surface temperature on the Greenland ice sheet, *Polarforschung, 59*, 113-128, 1991.

Richards, L.A., Capillary conduction of liquids through porous mediums, *Physics, 1*, 318-333, 1931.

Shapiro, R., Solar radiative flux calculations from standard meteorological observations, *Scientific Rep. 1*, Syst. and Appl. Sci. Corp., Riverdale, Md., (under contract to Air Force Geophys. Lab., *Rep. AFGL-TR-82-0039*), 1982.

Shapiro, R., A simple model for the calculation of direct and diffuse solar radiation through the atmosphere, *Scientific Rep. 35*, ST Syst. Corp., Lexington, Mass., (under contract to Air Force Geophys. Lab., *Rep. AFGL-TR-87-0200*), 1987.

Shimizu, H., Air permeability of deposited snow, *Contribution 1053* (English Translation), Inst. of Low Temperat. Sci., Sapporo, Japan, 1970.

Stephenson, P. J., Some considerations of snow metamorphism in the Arctic ice sheet in the light of ice crystal studies, *Physics of Ice and Snow, Proceedings of an International Conference on Low Temperature Science*, Inst. of Low Temperat. Sci., Hokkaido Univ., Sapporo, Japan, pp. 725-740, 1967.

Van der Veen, C. J., Ice sheets and the CO_2 problem, *Surv. in Geophys., 9*, 1-42, 1987.

Warrick, R., and J. Oerlemans, Sea level rise, in *Climate Change: The IPCC Scientific Assessment*, edited by J.T. Houghton, G. J. Jenkins, and J. J. Ephraums, pp. 257-281, Cambridge University Press, Cambridge, 1990.

R. Jordan, Geophysical Sciences Branch, U.S. Army Cold Regions Research and Engineering Laboratory, Hanover, NH 03755-1290. rjordan@hanover-crrel.army.mil.

K.C. Kuivinen. Snow and Ice Research Group, University of Nebraska-Lincoln, Lincoln, NE 68588-0135. kuivinen@unlinfo.unl.edu

C.M. Rowe, Meteorology/Climatology Program, Department of Geography, University of Nebraska-Lincoln, Lincoln, NE 68588-0135. crowe@unlinfo.unl.edu.

(Received September 7, 1994; revised April 5, 1995;
accepted April 19, 1995.)